MODELING THE EFFECTS OF LONGWALL MINING ON THE GROUND WATER SYSTEM[1]

by

R. J. Matetic[2], J. Liu[3], and D. Elsworth[4]

Abstract: The objective of this U.S. Bureau of Mines hydrologic/ subsidence investigation was to evaluate the effects of longwall mining on the local ground water regime through field monitoring and numerical modeling. Field data were obtained from multiple-position borehole extensometers (MPBX's) that were used to measure subsurface displacements. Survey monuments were installed to measure mining-induced surface deformations. Numerous drawdown and recovery tests were performed to characterize hydrologic properties of the overburden strata. Coreholes were drilled above the study area to determine lithologic and strength characteristics of the overburden strata using the rock samples collected. Electronic recorders were installed on all monitoring wells to continuously monitor ground water levels in coordination with mining of the longwall panels. A combined finite element model of the deformation of overlying strata, and it's influence on ground water flow was used to define the change in local and regional water budgets. The predicted effects of the postmining ground water system determined by the model correlated well with field data collected from the field site. Without an infiltration rate added to the model, a static decrease of 3.0 m (10 ft) in water level would occur due to mining of both longwall panels and if an infiltration rate was inputted in the model, no predicted long-term effects would occur to the ground water system.

Introduction

Longwall mining is a method used to extract large blocks of coal. During extraction of the block, the immediate overburden is allowed to collapse, filling the void created by the excavation. Mining-induced strains and displacements are transferred throughout the overburden rock mass due to this collapse and the resultant stress redistribution creates changes to the ground surface and any water-bearing zones located above the mining area. Previous studies have been conducted to delineate the effects of longwall mining on the local ground water system (Booth 1992; Elsworth 1994; Johnson 1992; Leavitt 1992; Matetic 1990; 1991, 1992; Tieman 1992; and Trevits 1991)). Few of these studies, however, have used actual field data, in conjunction with numerical modeling, to determine and

predict mining effects on the ground water regime. The U.S. Bureau of Mines (USBM) is studying the overburden rock mass and its response to high-extraction mining operations through a comprehensive program of field studies. The first part of the work involves the collection of mining, subsidence, overburden response, and hydrological data before, during, and subsequent to mining activity at numerous field sites. The second part of the program is examining methods of predicting the impact to local ground water supplies after mining activity occurs. One of these methods, is through the application of numerical modeling.

Model Approach

An intensive surface, subsurface, and ground water monitoring program was conducted at a mine site in southeastern Ohio. Data collected from this site served as input information for a Finite Element (FE) model. The two-dimensional FE model incorporates the deformation of overlying strata and its influence on ground water flow through applying a simple relationship between mining-induced strains and changes in hydraulic conductivity. The strain field that develops around a longwall panel as a result of mining is caused by material failure and self-weight. From this predicted strain field and from knowledge of the premining hydraulic properties of the overlying strata, the change in hydraulic conductivity that results from the strain field may be determined. With the modified conductivity field determined, the postmining hydrologic system may subsequently be defined through application of a ground water flow model. Again, this ground water model utilizes the finite element method to determine the postmining hydrologic system where the position of the piezometric surface indicates changes in well or aquifer yields. This methodology is used to evaluate the

influence of mining on the local ground water regime in this study.

Theoretical Analysis of Modeling Approach

The following assumptions are made when operating the model: (1) the rock matrix is functionally impermeable in comparison with fractures; (2) fluid flow in fractures is defined on the basis of the parallel plate model; (3) changes in fracture conductivity result from changes in normal strains only; (4) strains are partitioned between fractures and matrix as defined by a modulus reduction factor, R_m; and (5) fracture spacing, s, does not change after mining activity (Liu 1994 and Ouyang 1993).

Correlation of Induced Strain and Hydraulic Conductivity

The equivalent porous medium conductivity, K_o, of a rock mass containing a parallel set of fractures can be defined as:

$$K_o = \frac{g}{12 \nu_k} \frac{b^3}{s} \qquad (1)$$

where g is gravitational acceleration, ν_k is kinematic viscosity, b is the fracture aperture and s is spacing. R_m, the modulus reduction factor may be defined as:

$$R_m = \frac{E}{E_r} \qquad (2)$$

where E is the deformation modulus of the rock mass and E_r is the deformation modulus of a rock specimen. The modulus reduction factor, R_m, enables the closure across a fracture, Δu_j, to be determined from the difference between the strains in the rock mass and rock speciman as shown below:

$$\Delta u_j = [b + s (1 - R_m)] \Delta \epsilon \qquad (3)$$

97

where $\Delta\varepsilon$ is the strain in the direction perpendicular to the fracture plane. $\Delta\varepsilon$ is positive in extension and negative in compression.

Using the applied strain, $\Delta\varepsilon$, from above, the revised conductivity of equation (1) may be defined as:

$$K = R_c K_o \qquad (4)$$

where

$$R_c = \left| 1 + \frac{b + s(1 - R_m) b^3}{b} \right| \Delta\varepsilon \qquad (5)$$

Directional conductivities, evaluated from initial conductivities, K_{ox} and K_{oy} (conductivities in the x- and y-directions, respectively) may then be determined from equation (4). With two sets of orthogonal fractures oriented in the x and y directions, the revised directional conductivities may be defined for a two-dimensional system as:

$$= K_{xo} \left[1 + \frac{b + s(1 - R_m)}{b} \Delta\varepsilon \right. \qquad (6)$$

and

$$= K_{yo} \left[1 + \frac{b + s(1 - R_m)}{b} \Delta\varepsilon \right. \qquad (7)$$

where K_x and K_y are postmining conductivities in the x-direction and the y-direction, K_{xo} and K_{yo} are the premining conductivities in the x-direction and the y-direction, and $\Delta\varepsilon_x$ and $\Delta\varepsilon_y$ are the induced strains in the x and y directions, respectively. R_m is a modulus reduction ratio (ratio of mass modulus to intact modulus) that apportions the changes in strain between the fracture and matrix material. When $R_m = 1$, the mass modulus and intact material modulus are identical and the strain is uniformly distributed between fractures and matrix. This results in the smallest possible change in conductivity. When $R_m = 0$, the extensional strain is applied entirely to the fracture system and precipitates the largest possible change in conductivity. These values bound the possible ranges in the behavior of the system in a natural and mechanistically defensible manner. This representation of conductivities is extremely useful, since the modulus-reduction factor, R_m, may be readily evaluated from rock mass classification systems defining structural behavior as a function of readily observable factors of rock structure (Voight 1970). This avoids the difficulty of defining conductivity enhancement in terms of the component moduli of fractures and matrix, parameters that are unlikely to be available in practice. The mining-induced conductivity changes can then be evaluated through equations 6 and 7, provided the mining-induced strain field is determined.

Determination of the Strain Field

The subsidence field that develops around a longwall panel may be determined directly from the FE model. The finite element model applies gravitational load, removes material excavated from the panel and allows the overburden material to fail and deform according to the mining-induced strains. The resulting subsidence field may use the modulus reduction parameter, R_m, to calibrate against field data for a particular site. The insensitivity of the resulting subsidence profile to the material properties of deformation modulus and rock strength parameters, originates from the overriding influence of geometric controls on deformation (Stoner 1983 and Walker 1986). Following mining, the panel span is sufficiently large that closure between panel floor and roof is unavoidable.

98

Consequently, the resulting strain field, e_x and e_y is defined purely as a function of geometry, as:

$$e_x, e_y = f\left[\frac{w}{t}, \frac{w}{h}\right] \quad (8)$$

where: w represents the width of the panel, t is the thickness of the coalbed and h symbolizes the thickness of the overburden.

The assumption necessary in this evaluation is that strains are uniformly distributed at the scale of a single element. These assumptions seem reasonable where strains are moderate, but may be questionable where significant strain localization occurs.

Determination of the Postmining Ground Water Regime

With the modified conductivity distribution determined from an evaluation of the strain field, and equations (16) and (17), the influence on the postmining ground water regime may be evaluated. The finite element model may determine the influence of a continuously distributed conductivity field (evaluated from the calculated strain distribution) on the ground water budget and water table where boundary conditions are applied to the local system, to represent ground water and surface recharge. Therefore, the change in elevation of the phreatic surface may be determined for the postmining regime. This enables the influence of mining on well yields, aquifer yields, and flow patterns to be identified.

Input Parameters Used for
the Modeling Approach

The primary parameters used as input to the model and the measurements obtained from the field are: (1) the initial hydraulic conductivity distribution of the local lithology as determined through field measurements;

(2) modulus of elasticity and Poisson Ratio for the rock mass determined from field measurements; (3) the measured subsidence profile; (4) measured vertical displacements; (5) continuous fluid level fluctuations monitored at the site; and 6) flow rates entering the mine after excavation of the longwall panels, as recorded by the operator.

Site Description and Ground Water Monitoring Program

Site Description. The study site is located in southeastern Ohio (Vinton County). The study area overlies a portion of two contiguous longwall panels (Panel Nos. 1 and 2) measuring approximately 300 m (900 ft) wide and 2,950 m (9,000 ft) long (figure 1). The panels were separated by a five entry, four pillar system approximately 120 m (350 ft) wide. The mined coalbed, had an average thickness of 140 cm (55 inches) within the study area. However, the extraction thickness varied between 173 and 183 cm (68 and 72 inches). Overburden thickness was small and ranged from 65 to 85 m (214 to 280 ft). Overall, the strata were fairly level with a regional dip of about 1 degree towards the southeast. There were no major geologic structures and the topography consisted mainly of rolling hills with a maximum relief of approximately 49 m (160 ft).
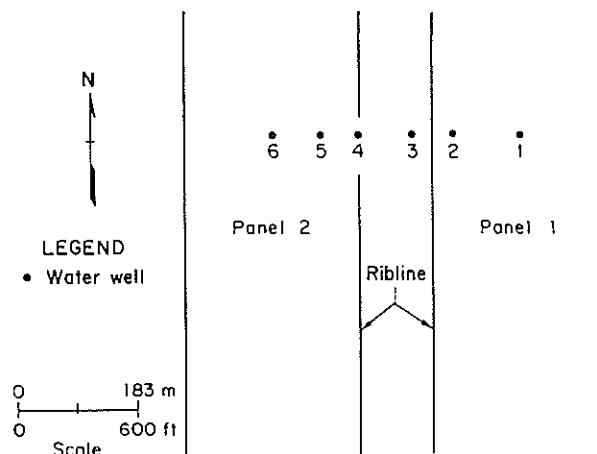

Figure 1. Sketch of study area.

99

Ground Water Monitoring Program. A total of seven 22-cm (8 5/8-in) diameter monitor wells were drilled for the study. Perforated Schedule 80 (15-cm diameter) (6-in) PVC casing was installed to the total depth in each well to ensure an open wellbore for the life of the study. The wells were strategically placed above both longwall panels as shown in figure 2. The wells were located along a line perpendicular to the trend of the longwall panels. This alignment permitted observations of effects during the mining of both longwall panels. Well Nos. 1 and 6 were located at the center of panel Nos. 1 and 2 respectively. Well Nos. 2 and 5 were located at quarter-panel width. Well No. 3 was located above the gate roads between the two panels and Well No. 4 was located above the edge of panel No. 2. Well No. 7, a control well, was located 427 m (1,400 ft) away from any mining activity.

Data was collected from all wells before, during, and after mining of both longwall panels. Various hydrologic parameters were determined and included specific capacity, transmissivity, hydraulic conductivity, and water level fluctuations. Initial data collection began three months prior to the undermining of Well No. 1 to establish baseline conditions. Drawdown and recovery pumping tests were performed on all wells before and after undermining to determine hydraulic conductivity parameters of the local, shallow geologic units.

Electronic recorders were also installed on all wells to continuously monitor water level fluctuations. The electronic data logger was programmed to record fluid positions every 4 hours.
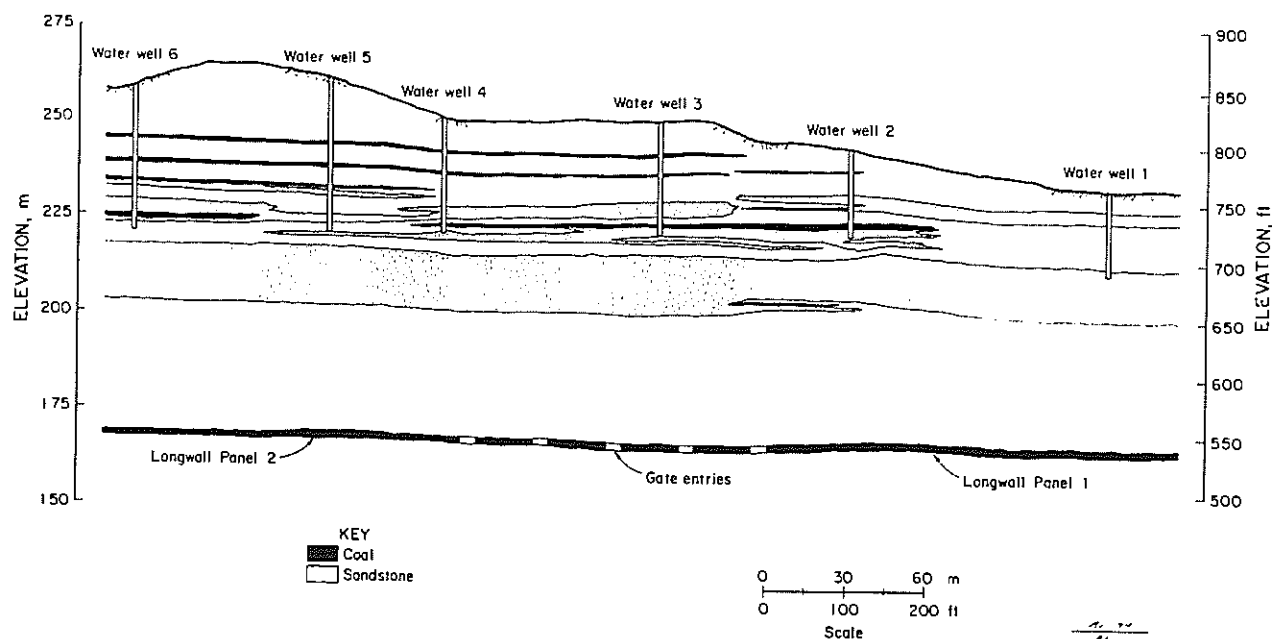

Figure 2. Generalized cross section of study area and Water Well locations

100

Geology

The geological setting of the study area is typical of that found in southeastern Ohio. The regional dip in this part of the state is to the southeast with the strata striking in a northeast-southwest direction. The average rate of dip is 6 m/km (30 ft/mi). Irregularities to this rate can be experienced by localized thinning or thickening of individual rock units (6). The rock is predominantly interbedded sandstones, shales, thin coal seams and claystones. The individual units are thin (less than 3 m (10 ft) thick) with one sandstone unit having an average thickness of 14 m (45 ft) and lying 43 m (140 ft) above the Clarion 4A Coalbed. To characterize overburden lithology prior to drilling the monitoring wells, six NX-sized coreholes were drilled in the study area to the Clarion 4A Coalbed. Generally, the overburden consisted of about 30% sandstone, 30% shale, 30% claystone, and 10% coal. A generalized cross-section of the study area with the monitor well locations is shown in figure 2.

Modulus of Elasticity and Poisson Ratio Values

The coreholes were drilled above the study area to characterize the local lithology of the overburden and to provide samples for determining geotechnical properties. For input to the model, tests for determining compressive strength, Modulus of Elasticity and Poisson Ratio were conducted on the rock cores collected. Results of tests performed on the core samples showed that the unconfined compressive strength of the major sandstone units are between 2.6×10^4 and 3.0×10^4 kg/m^2 (5,300 to 6,000 psi). Modulus of Elasticity and Poisson Ratio for these units are between 1.3×10^7 to 1.4×10^7 kg/m^2 (2.57 to 2.82×10^6 psi) and 0.30 to 0.32 respectively. A limestone unit,

averaging 2.1 m (7 ft) in thickness, is situated about 1 m (3 ft) above the mined coalbed. Testing of core samples show that the unconfined compressive strength of this unit is 1.2×10^5 kg/m^2 (25,000 psi), with a Modulus of Elasticity of 5.1×10^7 kg/m^2 (10.5×10^6 psi), and a Poisson Ratio of 0.28.

Overburden Deformation Monitoring Program

To observe overburden displacement, six 219.1 mm (8-5/8 in) boreholes were drilled along a profile line extending across the two longwall panels. Boreholes 1 and 6 were located in the center of each panel, where the maximum amount of subsidence was expected to occur. Boreholes 2 and 5 were located 30 m (91 ft) from the ribline inside each panel. Borehole 4 was situated 3 m (10 ft) from the ribline (inside the panel) in the expected zone of maximum horizontal tension. Borehole 3 was located in a pillar in the gate entries between the panels to observe the lateral extent of overburden deformation.

Each borehole was outfitted with an eight-anchor multiple-position borehole extensometer (MPBX). Two of the eight anchors in borehole 3 were installed inside a coal pillar to monitor yielding of the pillar. The anchors are numbered 1 to 8, with anchor 1 being the closest to the surface and anchor 8 being the deepest. Figure 3 displays MPBX and anchor locations with respect to the longwall panels.

Subsidence Monitoring Program

To obtain the field subsidence profile, survey monuments were installed on the ground surface and were surveyed regularly to identify the dynamic characteristics of subsidence, the final subsidence profile, and to provide surface reference data for the MPBX units. The monuments were constructed of 1.3 m (4 ft) rebar and

were installed flush to the ground surface. The array of monuments consisted of a baseline (along the centerline) over each panel and a profile line trending perpendicular between the two baselines. The monuments were spaced 15 m (45 ft) apart along the baseline. The profile line was 375 m (1,136 ft) long with monuments spaced 7.5 m (23 ft) apart.

MODEL ANALYSIS

Finite-element Mesh Assemblage

The finite-element mesh construction was assembled utilizing figure 3. The effects of topography, geometry, and lithology were incorporated in the mesh. The mesh utilizes uniform spacing and was constructed of 2,066 nodes and 1,928 elements. The mesh assumes differing materials (overburden material and coal layer) for the determination of strain and displacement characteristics, and three materials (upper shale layer, sandstone layer and lower shale layer) for determination of the postmining flow characteristics within the system. The boundary conditions of the model

for determining displacement and strain characteristics assume no horizontal movement on either side of the mesh and no vertical movement on the base. Boundary conditions associated with monitoring postmining ground water effects assume no flow on the bottom of the mesh and constant head conditions on the lateral sides of the mesh. The finite-element model is two-dimensional and determines the strain field with two displacement degrees of freedom applied to each node, and subsequently evaluates the revised flow system using a single degree of freedom. The analyses are coupled through the dependence of hydraulic conductivity on the induced strain field, as defined in equations 6 and 7.

Subsidence Profile

The subsidence profile (figure 4), generated by the model, was determined with the input parameters as shown in table 1.
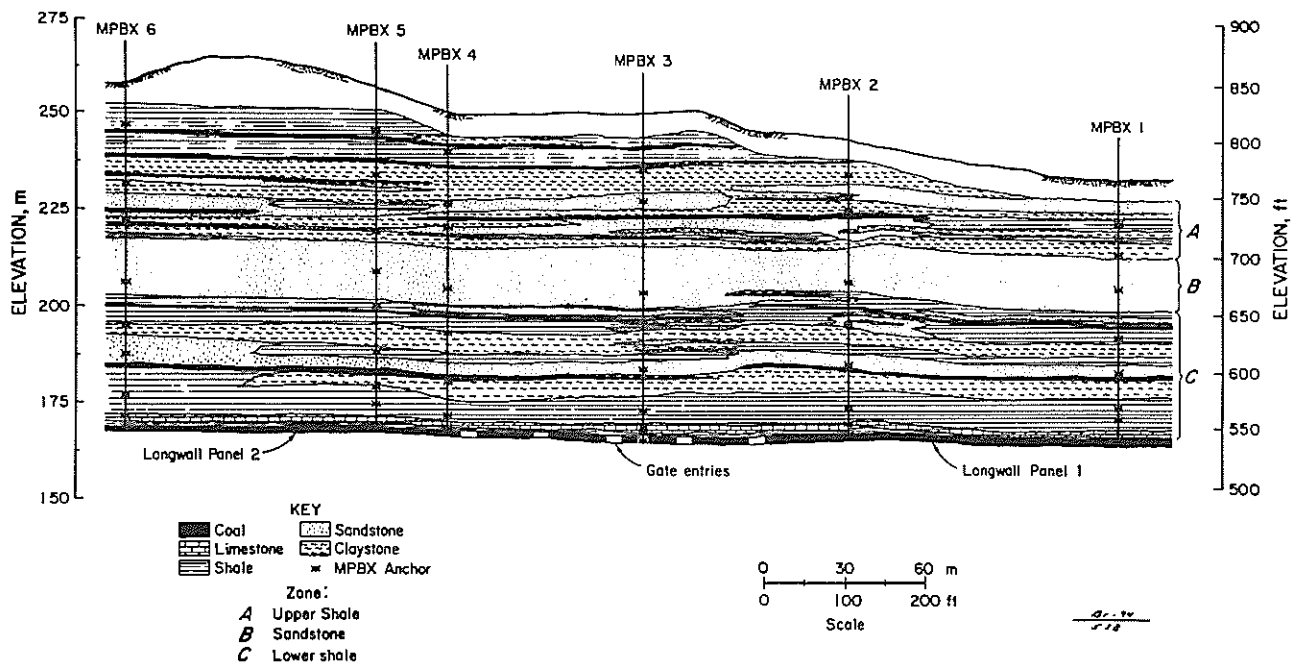

Figure 3. Generalized cross section of study area and MPBX locations
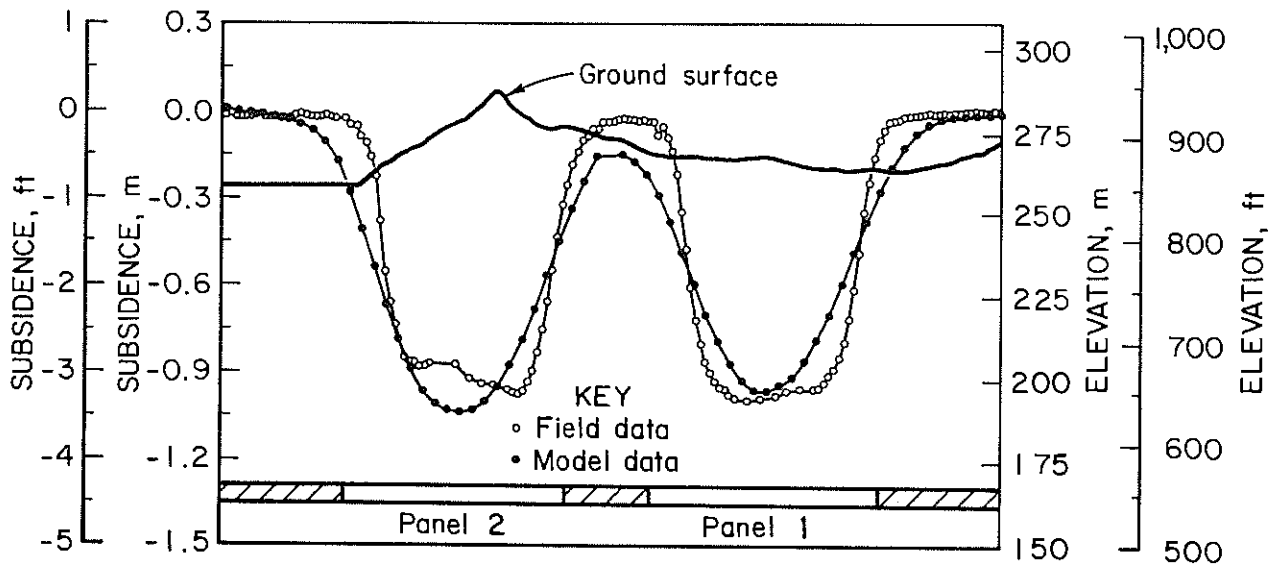
102

Figure 4. Comparison of field data and model subsidence profiles

Table 1.—Input parameters for generation of subsidence profile

Input Parameter	Overburden Material	Coal Layer
E, MPa (psi)	1,550 (2.2 x 10^5)	1.56 (2.2 x 104)
n	0.30	0.30
D, kg/m³ (lb/ft³) . .	2,400 (150)	390 (80)
E_{insitu}/E_{failed}	4.0	4.0
$n_{post\ failure}$	0.450	0.450

E = Modulus of Elasticity.
D = Density.
n = Poisson's ratio.

The values of the modulus of elasticity for the overburden were based on lab results obtained from core samples collected from the field site. To obtain the model inputs, an average of all field samples was calculated (3.0 x 10^9 kg/m² (6.4 x 10^8 lb/ft²)) and ratios of 1/20 for the overburden material and 1/200 for the coal material were applied to the average lab result. Prior research has shown that decreasing E_{lab} values by several orders of magnitude, results in a

better representation of actual field conditions and accounts for rock mass effects (Voight 1970). Voight (1970), has also noted that lab results within the range of 4.88 x 10^6 to 4.88 x 10^8 kg/m² (1.0 x 10^6 and 1.0 x 10^8 psi) should be reduced by at least one order of magnitude. A value of 4.0 was inputted into the model for the postfailure ratio of $E_{in\ situ}/E_{failed}$. This ratio is simply a curve fitting parameter to match the field-measured maximum subsidence magnitude with that

103

derived from the model. In reality, the form of the subsidence profile predicted by the model is insensitive to the choice of elastic parameters. The excavation of coal is simulated using a bimodulus model. Initially, this material is assigned a very small modulus and a Poisson Ratio equal to zero, allowing the material to freely deform in the vertical direction. As the top and bottom of the panel contact each other, the modulus of elasticity value is increased to prevent interpenetration.

Figure 4 shows the subsidence profile determined by the model and the actual subsidence profile obtained from the collected field data. Although the two curves are not identical, the general trends of the curves are similar, with the maximum subsidence located above the two panels. This match is considered adequate for the subsequent hydrologic analyses.

Comparison of Vertical Displacements Determined by the Model and Field Data

Strain distributions are determined in the finite element model by solving the boundary value problem with appropriate constitutive relations. The subsidence profile is the surface manifestation of this continuous redistribution of strain surrounding the mined panel. Strains and displacements generated within the mesh, as a result of mining, may also be determined and analyzed. A comparison of vertical displacements, within the overburden, as generated by the model and the displacements measured at the field site are shown in tables 2-4.

Table 2.—V_{field} versus V_{model} (vertical displacements) for MPBX nos. 1 and 2

Borehole	Anchor	Height		V_{field}		V_{model}	
		m	ft	m	ft	m	ft
1	1	54.56	179	1.14	3.73	1.00	3.28
	2	50.60	166	1.16	3.79	1.01	3.30
	3	47.00	154	1.17	3.85	1.01	3.30
	4	38.10	125	1.30	4.26	1.01	3.30
	5	25.91	85	1.50	4.90	1.01	3.30
	6	16.15	53	F	F	1.00	3.28
	7	8.53	28	F	F	1.00	3.25
	8	6.10	20	F	F	1.00	3.25
2	1	64.62	212	0.57	1.87	0.50	1.63
	2	57.91	190	0.57	1.87	0.50	1.63
	3	55.17	181	0.60	1.98	0.50	1.63
	4	38.71	127	0.70	2.27	0.51	1.68
	5	27.74	91	1.64	5.37	0.51	1.68
	6	18.59	61	F	F	0.52	1.71
	7	9.45	31	F	F	0.53	1.73
	8	5.18	17	F	F	0.53	1.74

F - Anchor Failed
A - Anchor Number

Table 3—V_{field} versus V_{model} (vertical displacements) for MPBX nos. 3 and 4

Borehole	Anchor	Height		V_{field}		V_{model}	
		m	ft	m	ft	m	ft
3 . . .	1	70.10	230	0	0	0.09	0.29
	2	60.35	198	0	0	0.07	0.23
	3	36.90	121	0	0	0.07	0.22
	4	16.70	55	0	0	0.07	0.24
	5	7.01	23	0	0	0.07	0.24
	6	2.44	8	0	0	0.07	0.24
	7	0.91	3	0	0	0.07	0.24
	8	0.30	1	0	0	0.07	0.24
4 . . .	1	70.71	232	0	0	0.30	0.99
	2	58.52	192	0	0	0..27	0.88
	3	52.73	173	0	0	0.25	0.82
	4	36.88	121	0	0	0.21	0.70
	5	25.30	83	0	0	0.19	0.62
	6	13.41	44	0	0	0.16	0.52
	7	3.96	13	0	0	0.14	0.47
	8	1.83	6	0	0	0.12	0.41

F - Anchor Failed
A - Anchor Number

Table 4 —V_{field} versus V_{model} (vertical displacements) for MPBX nos. 5 and 6

Borehole	Anchor	Height		V_{field}		V_{model}	
		m	ft	m	ft	m	ft
5 . . .	1	83.21	273	1.21	3.97	0.56	1.85
	2	64.00	210	1.28	4.20	0.56	1.85
	3	50.30	165	1.43	4.70	0.56	1.84
	4	39.62	130	1.44	4.73	0.56	1.85
	5	31.10	102	1.53	5.01	0.56	1.85
	6	19.2	63	F	F	0.59	1.93
	7	10.36	34	F	F	0.60	1.96
	8	5.80	19	F	F	0.61	1.99
6 . . .	1	75.60	248	1.09	3.56	1.10	3.62
	2	62.79	206	F	F	1.11	3.63
	3	51.21	168	1.10	3.62	1.12	3.66
	4	38.10	125	F	F	1.12	3.66
	5	27.43	90	F	F	1.11	3.64
	6	19.50	64	1.14	3.73	1.11	3.61
	7	9.45	31	F	F	1.09	3.57
	8	3.96	13	F	F	1.08	3.53

F - Anchor Failed
A - Anchor Number

The predicted vertical displacement data obtained from the model for MPBXs Nos. 1, 2, 3, and 6 correlate well with the field data collected at the site (tables 2-4). The field displacement data for MPBX No. 4 (table 3) showed minimal vertical displacement, whereas, the predicted vertical displacements for these boreholes showed slightly higher magnitudes of displacement (.07 to .30 m) (0.22 to 0.99 ft). One contributing factor could be the difference between the predicted subsidence profile and the actual field data (figure 4). As displayed in the figure, the field data profile shows minimal amounts of subsidence occurring above the gate roads between the two panels. Whereas, the predicted subsidence profile shows a maximum of 0.15 m (0.5 ft) subsidence.

The anchors in MPBX No. 5 displayed larger magnitudes of vertical displacements as compared to those predicted by the model. Again, this is mainly attributed to the differing shapes of the subsidence profiles above

the vicinity of the ribline over panel No. 2 (figure 4). The profile, developed from the model, shows less subsidence occurring above the ribline as compared to the profile determined from the field data. As shown in the figure, the maximum subsidence (field data) for panel No. 2 occurs near the ribline, whereas, the model predicted maximum subsidence to occur above the center of the panel. This nonclassical form of the subsidence profile is attributed to site-specific geological conditions that are undefined and therefore not incorporated into the homogeneously distributed material parameters used in the finite element evaluation of displacements.

Correlation of the Postmining Hydrologic Regime with Data Collected from Field Site

The postmining effects to the ground water system (figure 5), evaluated from the model, were determined though input of the parameters as shown in table 5.

Table 5.—Input parameters for determination of postmining ground water effects

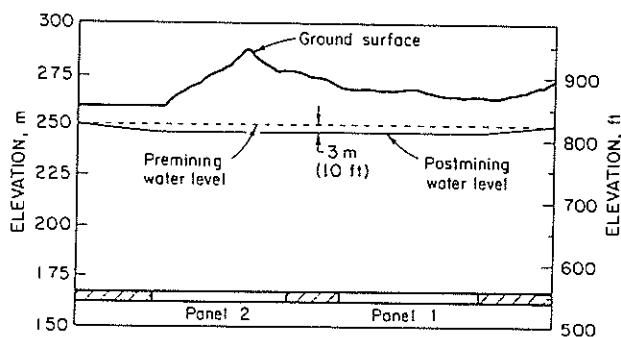| Input Parameter	Overburden Upper Shale	Overburden Sandstone	Overburden Lower Shale
K_x, Horizontal Conductivity	7.01×10^{-8} m/s (2.3×10^{-7} ft/s)	7.01×10^{-5} m/s (2.3×10^{-4} ft/s)	7.01×10^{-9} m/s (2.3×10^{-8} ft/s)
K_y, Vertical Conductivity	7.01×10^{-8} m/s (2.3×10^{-7} ft/s)	7.01×10^{-5} m/s (2.3×10^{-4} ft/s)	7.01×10^{-9} m/s (2.3×10^{-8} ft/s)
S, Fracture Spacing	0.31 m (1 ft)	0.91 m (3 ft)	0.10 m (0.30 ft)
R_m, Modulus Reduction Factor	0.80	0.05	0.97
ν, Kinematic Viscosity	1.0×10^{-6} m²/s (1.0×10^{-5} ft²/s)	1.0×10^{-6} m²/s (1.0×10^{-5} ft²/s)	1.0×10^{-6} m²/s (1.0×10^{-5} ft²/s)
g, Acceleration of Gravity	9.81 m/s² (32.2 ft/s²)	9.81 m/s² (32.2 ft/s²)	9.81 m/s² (32.2 ft/s²)
I, Infiltration Rate	0.23 m/yr (0.75 ft/yr)	0	0

Figure 5. Postmining effects of ground
water system - predicted by model.
Flow rate - Q = 2,390 Lpm (630 gpm)

Numerous drawdown and recovery
pumping tests were performed on all of
the monitoring wells to determine
hydraulic conductivity values. The
hydraulic conductivity value of the
7.01 x 10^{-8} m/s (2.3 x 10^{-7} ft/s), upper
overburden material (shale), for input
to the model, was determined by
averaging the hydraulic conductivity
values measured at the site. The
estimated hydraulic conductivity value,
7.01 x 10^{-5} m/s (2.3 x 10^{-4} ft/s) for the
sandstone material was used as input
into the model. This value was 3
orders of magnitude greater than the
measured conductivity value obtained
for the upper overburden material.
This value of hydraulic conductivity
was used because it is believed that
the sandstone unit provides a much
higher permeability than that of a
shale unit. The hydraulic conductivity
for the lower overburden material
(shale) was one order of magnitude less
than that of the upper material 7.01 x
10^{-9} m/s (2.3 x 10^{-8} ft/s). Prior USBM
research has shown that fractures
within the overburden rock mass
commonly decrease in aperture and
number with increasing depth (Walker
1986). Correspondingly, the rock mass
at depth is assumed 'tighter' and
consequently less conductive.

The fracture spacing values used
are assumed, since no information
regarding fracture spacings were
determined at the field site. However,
the selected values are consistent with
those incorporated in other successful
calibration studies (Elsworth 1994, Liu
1994, and Ouyang 1993). As mentioned
earlier, the modulus reduction factor,
R_m, reflects the partitioning of mining-
induced strains between fractures and
the porous matrix. In less stiff
materials, the matrix accommodates
proportionately more of the applied
bulk strain than stiffer materials,
where fracture closure dominates the
mass response. Correspondingly, less
competent materials, such as shales,
return higher magnitudes of the modulus
reduction factor. In the absence of
field measured magnitudes, appropriate
magnitudes of the modulus reduction
factor are selected, reflecting these
anticipated characteristics of
behavior.

Flow rates entering the mine
following the excavation of both panels
were monitored by the mining company.
Mine personnel estimated flow rates
through the monitoring of a main sump
located underground. Effects of
surface area, lithology, and
hydrogeology were incorporated into the
analysis to determine flow rate
estimates. This information provided a
reasonable basis for the selection of
several values for input into the model
i.e., fracture spacing (s) and modulus
reduction factor (R_m). The flow rate
provided by the mining company was
approximately 2,390 lpm (630 gpm).
Values of R_m, determined through
matching the flow rate, were 0.80 for
material 1, 0.05 for material 2, and
0.97 for material 3. Choice of these
parameters was clearly non-unique, but
was predicted on the anticipated
response of the lithologic units to
straining and fracturing. The pre-
existing fractures in the upper shale
and the lower shale units have less
effects on the postmining
conductivities than those in the

107

sandstone layer unit. Actually, the shale material may be treated as a porous medium which is not sensitive to deformation. The difference between the two values is due to the effect of depth. The value of R_m is chosen as 0.05 for the sandstone unit because a large part of the extensional strain is applied to the fracture system and precipitates the largest possible change in conductivity.

The coarse finite element mesh, used to evaluate the subsidence profile and overburden displacements, was applied to determine the influence of mining-induced permeability changes on the ground water system. The predicted effects on the postmining ground water system determined by the model correlated well with the field data collected at the site as shown in figures 6-11. Figures 6-11 show water level fluctuations measured for Well Nos. 1-6, respectively. In addition, curves were added to the figures which show progression of the longwall face as a function of the overburden thickness. These values are expressed as the ratio of face position (FP) to overburden thickness (OB). For example, consider a longwall face that is moving towards a well but is 183 m (600 ft) away and the overburden at the site of the well is 61 m (200 ft). The FP/OB ratio is - 3. The negative value of FP/OB ratio indicates a premining position of the longwall face; zero indicates when the respective longwall face passed beneath the line of wells; and a positive value indicates postmining positions of the longwall face past the line of wells. If at another site a longwall face was approaching a well but was 366 m (1,200 ft) away and the thickness of the overburden at the site of the well was 122 m (400 ft), the FP/OB ratio is still -3. This curve allows one to compare well response at two different sites (conceivably in the same study area) without having too make complicated adjustments for differing overburden thicknesses. Under the

applied boundary conditions, the model determined that a static decrease of 3.0 m (10 ft) in water level would occur due to the mining of both longwall panels. It should also be noted, that this decrease would occur without an infiltration rate inputted in the model. If an infiltration rate of 0.23 m/yr (0.75 ft/yr) is used, the regional model predicts that essentially no effects to the static phreatic surface would result. This infiltration rate is 25% of the total precipitation occurring at the site and correlates well with known infiltration rates of previous studies (Stoner 1983). Precipitation records provided by the mining company showed an average precipitation of 0.91 m (3.0 ft) which occurred at the site. Therefore, an infiltration rate of 0.23 m/yr (0.75 ft/yr) was used. Figure 5 shows the model prediction after excavation of both longwall panels.
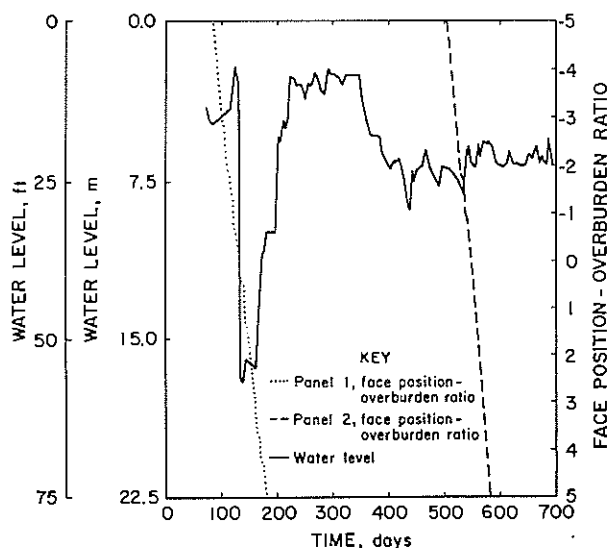

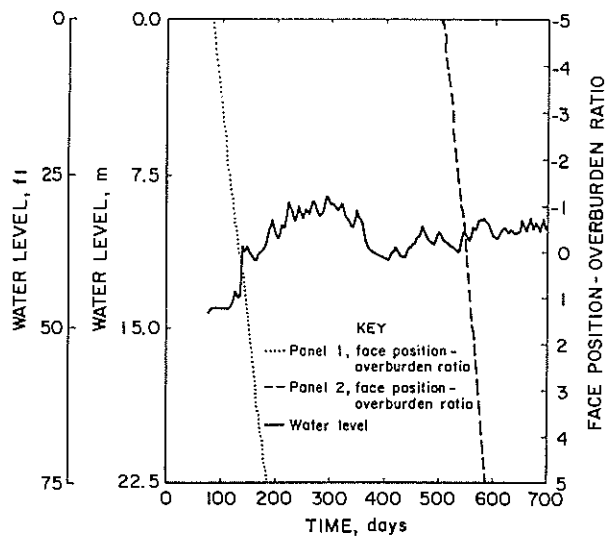Figure 6. Comparison of water level change and face position to overburden ratio for Well 1

Figure 7. Comparison of water level
change and face position to
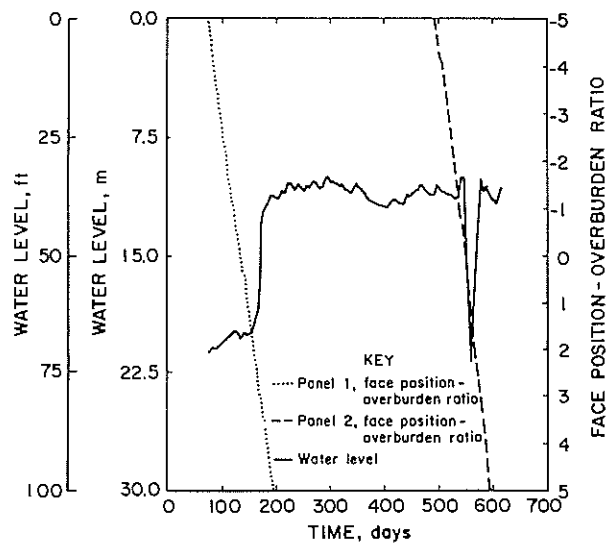overburden ratio for Well 2

Figure 9. Comparison of water level
change and face position to
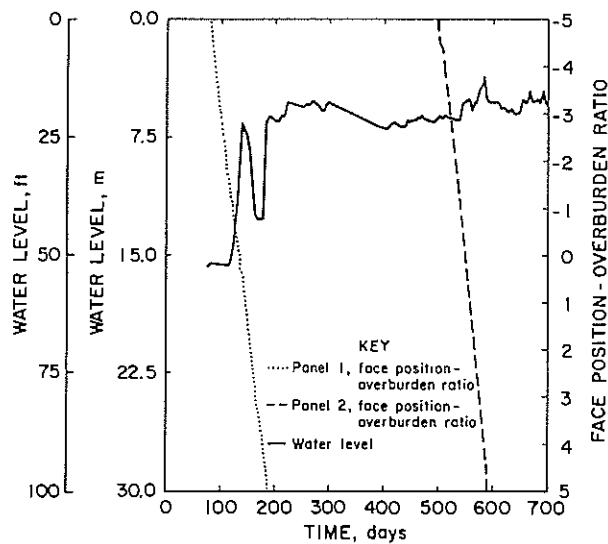overburden ratio for Well 4

Figure 8. Comparison of water level
change and face position to
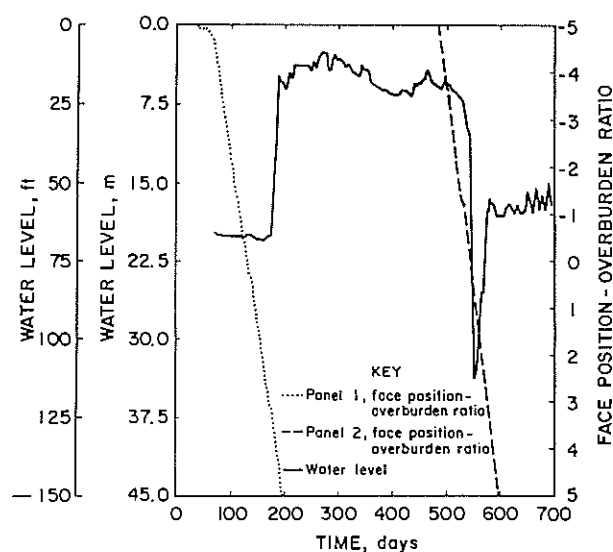overburden ratio for Well 3

Figure 10. Comparison of water level
change and face position to
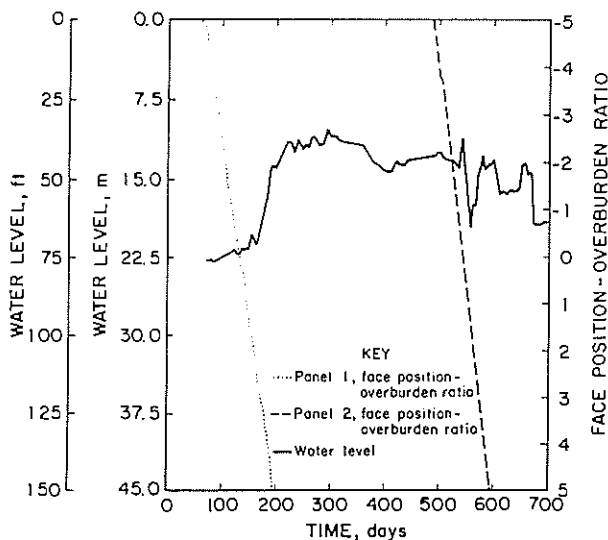overburden ratio for Well 5

109

Figure 11. Comparison of water level
change and face position to
overburden ratio for Well 6

In addition to applying the
regional model, described above, local
behavior around the shallow well field
(figure 12a) was also represented by a
more refined model to accommodate more
subtle water budget changes as a result
of mining. The changes in hydraulic
conductivities predicted from the
initial calculations were applied to
the zonation as defined in figure 12b.
These zones represent average changes
in hydraulic conductivities evaluated
from the subsidence modeling. The
refined mesh is capable of accurately
representing local changes in the
location of the phreatic surface. This
mesh represents the region between the
centerlines of both panels containing
well nos. 5 and 6 within Zone I, well
nos. 2-4 within Zone II, and well no. 1
within Zone III. No flow boundary
conditions were specified along the
base and on the left side (the
centerline of panel No. 2) and constant
head conditions were applied on the
remaining vertical side (about 76.2 m
(250 ft) away from the centerline of
panel No. 1). The mesh, utilized
uniform spacing, and was constructed of
326 nodes and 295 elements. Two
different situations were simulated

through use of the refined mesh. Fist,
the same infiltration rate and
premining ground water conditions were
inputted, where the small-scale
influences of topographically induced
flow were accommodated. Secondly, the
postmining hydraulic conductivity
magnitudes of table 5 were incorporated
to determine the anticipated postmining
ground water levels. The magnitude of
hydraulic conductivities were evaluated
directly from the spatial distribution
of strains, using equations 6 and 7.
Average magnitudes of horizontal and
vertical conductivities were then
utilized in the refined model of
figure 12. The changes in hydraulic
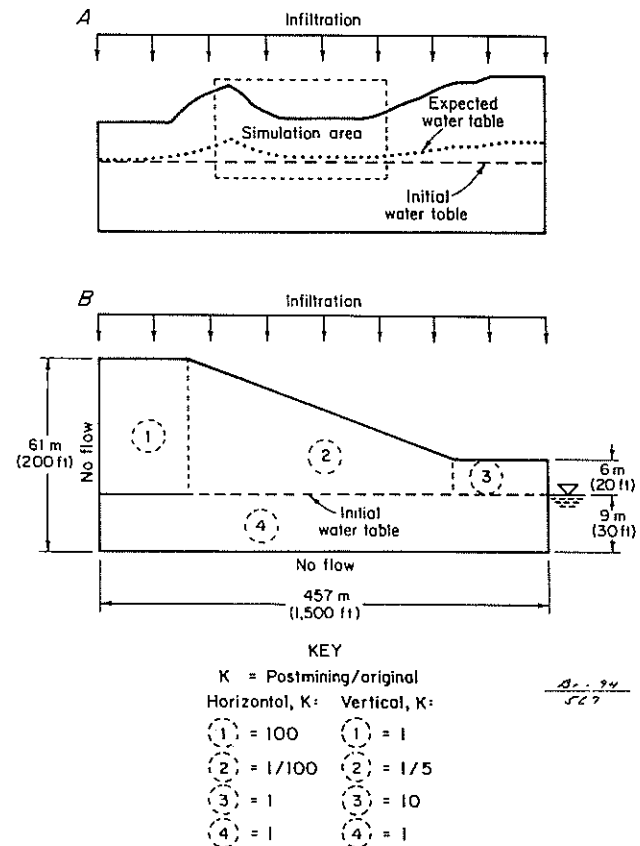conductivities are documented in
table 6.

Figure 12. Model for topographic
influence of infiltration on well
elevations. A, comceptual;
B, numerical

110

Table 6. Relative changes in
hydraulic conductivity
$(K_{postmining}/K_{original})$ as applied
to the small-scale mesh

Zone	K_h	K_v
1	100	1
2	1/100	1/5
3	1	10
4	1	1

K_h = Horizontal conductivity.
K_v = Vertical conductivity.

The resulting postmining
modification in the location of the
phreatic surface is illustrated in
figure 13. The subtle changes result
from applying the same infiltration
rate as used in the previous model run,
however, the greater element density of
this revised model highlights the
influence of even minor topography and
moderate changes in near surface
hydraulic conductivities on the ground
water system. The mining-induced
development of hydraulic conductivities
is such that water levels in the region
of wells 5 and 6 remain the same, water
levels in the region of wells 3 and 4
rise, and water levels in the region of
wells 1 and 2 fall, relative to
premining water levels. When the long-
term recorded levels in these six wells
are corrected relative to the control
well (a well located approximately
425 m (1,400 ft) away from mining
activity), this distribution of
behavior, and of this magnitude is
exactly as observed from the field
measurements performed at the site
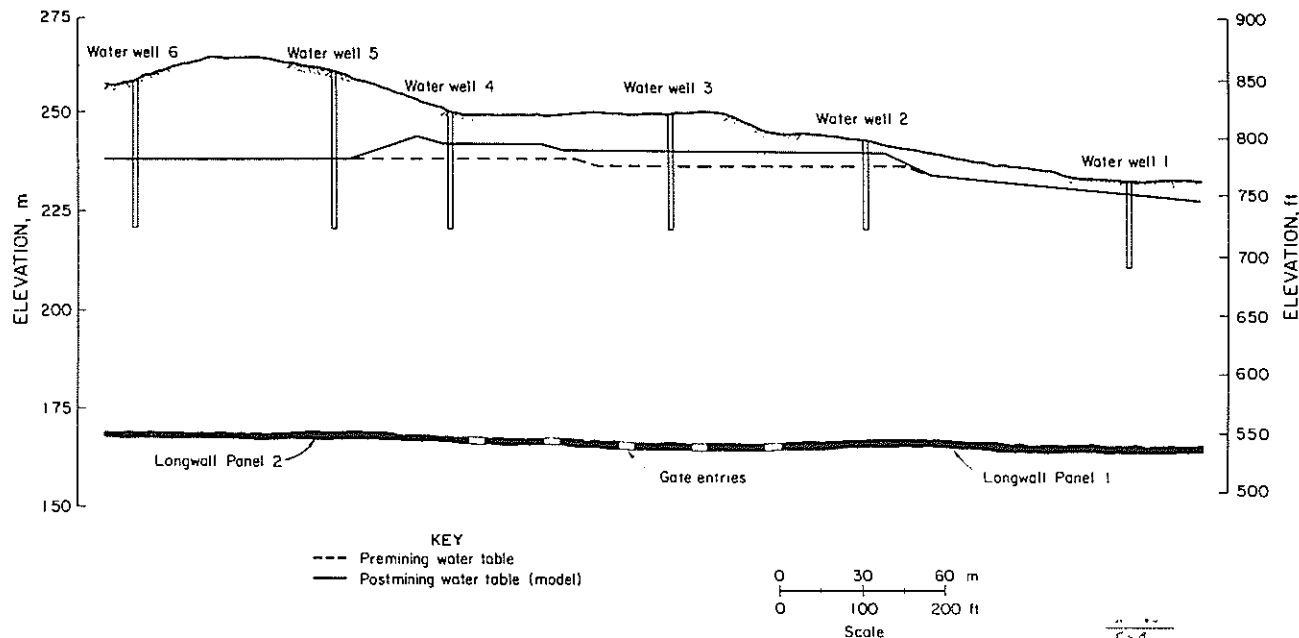(Matetic 1991) and as shown in
figures 6-11.

Figure 13.   Postmining effects on ground water system using
smaller-scale mesh around well area

111

Summary

1. The subsidence profile, as determined from the model, compares favorably with maximum subsidence measured at the field site.

2. The field data showed that minimal subsidence occurred above the gate roads between the two panels, while the predicted subsidence profile showed a maximum of 0.15 m (0.5 ft) subsidence at this location.

3. The predicted vertical displacement data obtained from the model for MPBX's Nos. 1, 2, 3, and 6 correlated well with the field data.

4. The field displacement data for MPBX No. 4 displayed minimal displacements, whereas, the predicted displacements for these boreholes showed slightly higher displacement. Also, MPBX No. 5 showed similar vertical displacements as compared to that predicted by the model.

5. The predicted effects of the postmining ground water system determined by the model correlated well with the field data collected at the site. Without infiltration added, the model determined that a static decrease of 3.0 m (10 ft) in water level would occur at the site due to the mining of both longwall panel nos. 1 and 2. If an infiltration rate was input to the model, no predicted effects for the long term would occur to the ground water regime which correlates well with field observations.

6. Where a fine mesh is used to define local changes in water budget within the well field area, the model is capable of replicating relatively subtle changes in long-term water levels. Minor local changes in the phreatic surface are consistent with the rolling topography of the site and the effects of mining-induced changes in hydraulic conductivity.

Conclusion

For this study, the numerical modeling results correlate favorably with the field data collected at the site. The surface subsidence information from the field, provided an excellent foundation for the modeling routine. If this information is not available, one should obtain and examine available subsidence prediction models to determine the profile information for the site. The assumptions made during the course of operating the model were based on knowledge of the subject area, experience with the model and insight gained from field tests. Again, if the field information is not available, the model routine requires some additional assumptions. Although a favorable correlation exists between the mining effects predicted and the field data collected, the authors feel that additional comparative studies at research sites with varying geology, longwall panel characteristics (thickness, width, etc.), hydrogeology, etc. should be performed to further substantiate the capabilities of the model.

References

Booth, C. J. Hydrogeologic Impacts of Underground (Longwall) Mining in the Illinois Basin. Paper in Procs. of the 3rd Workshop on Surface Subsidence Due to Underground Mining, Morgantown, WV, June 1-4, 1992, WVU, 1992, pp. 222-227.

Elsworth, D., Liu, J. and Z. Ouyang.
Some Approaches to Determine the
Potential Influence of Longwall
Mining on Ground Water Resources.
Paper in Procs. of the Inter-
national Land Reclamation and Mine
Drainage Conference and Third
International Conf. on the
Abatement of Acidic Drainage,
Pittsburgh, PA, April 24-29,
1994), Vol 4 of 4, NTIS, 1994, pp.
172-179.

Johnson, K. L. Influence of Topography
on the Effects of Longwall Mining
on Shallow Aquifers in the
Appalachian Coalfield. Paper in
Procs. of the 3rd Workshop on
Surface Subsidence Due to
Underground Mining, Morgantown,
WV, June 1-4, 1992, WVU, 1992, pp.
197-203.

Leavitt, B. R. and J. F. Gibbens.
Effects of Longwall Coal Mining on
Rural Water Supplies and Stress
Relief Fracture Flow Systems.
Paper in Procs. of the 3rd
Workshop on Surface Subsidence Due
to Underground Mining, Morgantown,
WV, June 1-4, 1992,. WVU, 1992,
pp. 228-235.

Liu, J. Topographic Influence of
Longwall Mining on Water Supplies.
M.S. Thesis, The Pennsylvania
State University, University Park,
PA, 1994, 73 pp.

Matetic, R. J., M. A. Trevits, and
T. Swinehart. A Case Study of
Longwall Mining and Near-Surface
Hydrological Response. Paper in
Procs. of the 1991 American Mining
Congress Coal Convention,
Pittsburgh, PA, June 2-5, 1991,
AMC, 1991, pp. 445-472.

Matetic, R. J. and M. A. Trevits.
Longwall Mining and its Effect on
Ground Water Quantity and Quality
at a Mine Site in the Northern
Appalachian Coalfield. Paper in
Procs. of the FOCUS Conference on
Eastern Regional Ground Water
Issues, Newton, MA, October 13-
15, 1992, Water Well Journal
Publishing Company, 1992, pp.
573-587.

Matetic, R. J. and M. A. Trevits. Case
Study of Longwall Mining Effects
on Water Wells. Paper in Procs.
of the SME Annual Meeting, Salt
Lake City, UT, Feb. 26-Mar. 1,
1990, SME preprint 90-141, 1990,
7 pp.

Ouyang, Z. and D. Elsworth. Evaluation
of Groundwater Flow into Mined
Panels. International Journal of
Rock Mechanics, Mineral Sciences
and Geomechanics, V. 30, No. 2,
1993, pp 71-79.

Stoner, J. D. Probable Hydrologic
Effects of Subsurface Mining.
Ground Water Monitoring Rev.,
Winter 1983, pp. 128-138.

Tieman, G. E. and H. W. Rauch. Study
of Dewatering Effects at a
Longwall Mine in Northern West
Virginia. Paper in Procs. of the
3rd Workshop on Surface
Subsidence Due to Underground
Mining, Morgantown, WV, June 1-4,
1992, WVU, 1992, pp. 214-221.

Trevits, M. A. and R. J. Matetic. A
Study of the Relationship Between
Saturated Zone Response and
Longwall Mining-Induced Ground
Strain. Paper in Procs. of the
5th Outdoor Action Conference on
Aquifer Restoration, Ground Water
Monitoring and Geophysical
Methods, Las Vegas, NV, May 13-
16, 1991, Water Well Journal
Publishing . Company, 1991, pp.
1101-1109.

Voight, B. and W. Pariseau. State of Predictive Art in Subsidence Engineering. Journal of Soil Mechanics and Foundations Division, V. 96, No. SM 2, 1970, pp. 721-750.

Walker, J. S., J. B. Green, and M. A. Trevits. A Case Study of Water Level Fluctuations Over a Series of Longwall Panels in the Northern Appalachian Coal Region. Paper in Procs. of the 2nd Workshop on Surface Subsidence Due to Underground Mining, Morgantown, WV, June 9-11, 1986, WVU, 1986, pp. 264-269.